JOURNAL OF CATALYSIS **160,** 190–204 (1996)
ARTICLE NO. 0138

Non-Faradaic Electrochemical Modification of Catalytic Activity

X. Ethylene Epoxidation on Ag Deposited on Stabilized ZrO_2 in the Presence of Chlorine Moderators

Ch. Karavasilis, S. Bebelis, and C. G. Vayenas

Department of Chemical Engineering, University of Patras, GR-26500 Patras, Greece

Received April 6, 1995; revised January 16, 1996; accepted January 18, 1996

The effect of non-Faradaic electrochemical modification of catalytic activity (NEMCA), or *in situ* controlled promotion was investigated during ethylene epoxidation on Ag films deposited on yttria-stabilized zirconia at temperatures from 240 to 300°C and 500 kPa total pressure in the presence of chlorinated hydrocarbon moderators. It was found that the rates of epoxidation and complex oxidation change by a factor of 230 as the catalyst potential and work function are varied by 0.6 V and 0.6 eV, respectively. The change in the total reaction rate is typically a factor of 100 higher than the rate $I/2F$ of electrochemical supply or removal of promoting oxide ions. The selectivity to ethylene oxide can be varied between 0 and 78% by varying the catalyst potential and dichloroethane partial pressure. At low catalyst potentials acetaldehyde becomes the main product with a selectivity up to 55%. The observed behavior is discussed on the basis of previous NEMCA studies and of the prevailing ideas about the mechanism of ethylene epoxidation. © 1996 Academic Press, Inc.

INTRODUCTION

Due to its industrial importance the ethylene epoxidation on silver is one of the most thoroughly studied catalytic systems (1–4). Work prior to 1987 has been reviewed by van Santen and Kuipers (4).

It is now firmly established that atomically chemisorbed oxygen is responsible for both the epoxidation and the complete oxidation reactions (4–10). Molecularly adsorbed oxygen has been shown by Lambert and co-workers to behave as a spectator species (5, 6). The product selectivity is governed by the binding state of atomic oxygen (4). Weakly bonded, electrophilic, atomic oxygen reacts preferentially with the double bond of adsorbed ethylene producing epoxide (4, 5, 11–13). Strongly bonded, bridging atomic oxygen coordinated to Ag atoms of low charge reacts preferentially with the hydrogen atoms of adsorbed ethylene, leading to CO_2 formation (4, 5, 11–13). The presence of subsurface oxygen (14–18) favors the formation of weakly adsorbed oxygen, thus increasing the selectivity to ethylene oxide (4, 18).

The effect of non-Faradaic electrochemical modification of catalytic activity (NEMCA) (19, 20), or electrochemical promotion (21), or *in situ* controlled promotion (22) has been described for over 30 catalytic reactions on Ag, Pt, Pd, Rh, IrO_2, Ni, and Au surfaces using O^{2-}, F^-, Na^+, and H^+ conducting solid electrolytes and more recently on aqueous KOH solutions (22–40). The importance of NEMCA in heterogeneous catalysis and electrochemistry has been discussed by Pritchard (21) and Bockris (41).

The porous catalyst film is deposited on a solid electrolyte such as yttria (8 mol%) stabilized zirconia (YSZ), an O^{2-} conductor, and also acts as an electrode in the following cell: gaseous reactants, catalyst $|ZrO_2(Y_2O_3)|$ counter electrode, air.

By externally applying currents or potentials between the catalyst and the counter electrode, ions ($O^{\delta-}$, $Na^{\delta+}$, F^-, or H^+ depending on the solid electrolyte) migrate (backspillover) onto the catalyst surface, as recently confirmed by *in situ* XPS (42). These backspillover ions act as promoters. The increase in the rate of the catalytic reaction is up to 100 times larger than the open-circuit (unpromoted) catalytic rate (37) and up to 3×10^5 times larger than the rate of ion supply (23). The effect is quite reversible and does not appear to be restricted to any type of reaction, metal catalyst, or solid electrolyte. The NEMCA literature and theory have been reviewed recently (22, 43–45).

The enhancement factor or Faradaic efficiency Λ is defined from

$$\Lambda = \Delta r/(I/2F), \qquad [1]$$

where Δr is the change in the catalytic reaction rate (expressed in mol O), I is the applied current (defined positive when anions are supplied to the catalyst), and F is the Faraday constant. A reaction exhibits the NEMCA effect when $|\Lambda| > 1$. When $\Lambda > 1$ the reaction is termed electrophobic (22, 24) and when $\Lambda < -1$ the reaction is termed electrophilic (22, 24). As shown both theoretically (22, 23) and experimentally (22–27) the order of magnitude of $|\Lambda|$

0021-9517/96 $18.00

can be estimated for any catalytic reaction from

$$|\Lambda| \approx 2Fr_o/I_0, \quad [2]$$

where r_o is the open-circuit (unpromoted) catalytic rate and I_0 is the exchange current (22, 46) of the catalyst–solid electrolyte interface. This parameter is measured from standard current–overpotential (Tafel) plots. Faradaic efficiency Λ values between -10^4 and $+3 \times 10^5$ have been measured (22–40, 43–45).

The rate enhancement ratio ρ is defined from

$$\rho = r/r_o, \quad [3]$$

where r is the NEMCA induced, i.e., promoted, catalytic rate; ρ values up to 100 (37, 43–45) and down to 0.5 (22, 43–45) have been measured using O^{2-} conducting solid electrolytes. Very recently Lambert and Harkness obtained ρ values approaching "infinity" during NO reduction by C_2H_4 on Pt/β''–Al_2O_3 (a Na^+ conductor) as the open-circuit, i.e., unpromoted, rate was practically nil (38). At the other extreme Cavalca and Haller (39) obtained ρ values approaching zero for benzene hydrogenation on Pt/β''–Al_2O_3. Sodium coverages of less than 0.1 were found to completely poison the rate.

The promotion index P_i is defined from

$$P_i = \frac{\Delta r/r_o}{\Delta\theta_i}, \quad [4]$$

where θ_i is the coverage of the promoting surface species on the catalyst metal M (e.g., $O^{\delta-}$–$M^{\delta+}$, $Na^{\delta+}$–$M^{\delta-}$); P_i values up to 250 and down to -50 have been measured (22–40, 43–45).

The Ag-catalyzed ethylene expoxidation is the first reaction for which a non-Faradic rate enhancement was found and Λ values up to 300 were measured (47, 48). Subsequent detailed atmospheric pressure investigations utilizing a third (reference) electrode (26) confirmed that both ethylene epoxidation and complete oxidation are predominantly electrophobic reactions and that the selectivity to ethylene oxide can only be moderately improved over the open-circuit (unpromoted) value. These previous studies (26, 47, 48) were limited to atmospheric pressure and high temperatures ($T > 350$°C) so that the selectivity was below 52%.

The present study, as well as a parallel NEMCA study of ethylene epoxidation on Ag/β''–Al_2O_3 (49), aimed at selectivity maximization by mimicking the industrial operating conditions (1–4, 50), i.e., by employing

(a) low operating temperatures (240 to 300°C),
(b) high operating pressure (500 kPa),
(c) gas-phase addition of chlorinated hydrocarbon moderators.

The NEMCA investigation of the present system gave ethylene oxide selectivities up to 78% for mildly negative catalyst potential (−0.16 V) and, surprisingly, acetaldehyde selectivities up to 55% for lower (−0.6 V) catalyst potentials. The parallel study on Ag/β''–Al_2O_3 gave ethylene oxide selectivities up to 88% (49).

EXPERIMENTAL

The apparatus utilizing on-line gas chromatography, mass spectrometry, and IR spectroscopy has been described previously (22–26).

Reactants were Messer Griesheim and L' Air Liquide certified standards of C_2H_4 in He, O_2 in He, and 1,2-dichloroethane in He (30 ppm). They could be further diluted in ultrapure (99.999%) He (L' Air Liquide).

The gas chromatographic analysis was carried out using a Shimadzu 14A gas chromatograph with a TC and an FI detector and a Perkin-Elmer LCI-100 computing integrator. A Porapak N packed column (80/100, $8' \times 1/8''$) was used to separate O_2, CO_2, and C_2H_4 at 70°C, as well as C_2H_4O, CH_3CHO, and H_2O at 150°C. The O_2 concentration was also measured using a Molecular Sieve 5A packed column (80/100, $8 \times 1/8''$) at 70°C and was continuously monitored in the exit stream by means of a Teledyne 326 RA oxygen electrochemical analyzer. The concentration of CO_2 in the product stream was also monitored using on-line IR spectroscopy (Foxboro 973 Miran analyzer). The carbon mass balance closure in all runs was better than 2%. No coking of the catalyst was detected. The only detectable products were CO_2, C_2H_4O, H_2O, and CH_3CHO. The inlet concentration of 1,2-$C_2H_4Cl_2$ in the gas phase was computed by measuring the individual flow rate of each certified gas mixture supplied to the reactor. Care was taken so that the pressure just before the mixing point was the same for each individual gas stream, in order to avoid any mistakes in the calculation of the 1,2-$C_2H_4Cl_2$ concentration. A Balzers QMG 311 mass spectrometer was also used to follow rate transients.

The YSZ continuous flow reactor shown in Fig. 1 has been described previously (22–26). It has a volume of 30 cm^3 and has been shown to behave as a CSTR in the flow rate range of the present investigation, i.e., 20–40 (cm^3 STP/min) (51, 52). Previous NEMCA studies in this type of reactor have been limited to atmospheric pressure operation (26, 47, 48). In the present study the reactor was operated as a continuous flow reactor (CSTR) at 500 kPa (~5 atm). The conversion of ethylene was kept below 5% both under open-circuit and closed-circuit conditions, i.e., the reactor was operated as a differential one. The rate of ethylene oxide oxidation was thus kept to negligible levels (51, 52).

The porous Ag catalyst film was deposited on the inside bottom wall of the YSZ tube by application of a thin coating of Ag paste (silver solution in butyl acetate, GC Electronics silver print 22-201), followed by drying at 60°C and calcin-

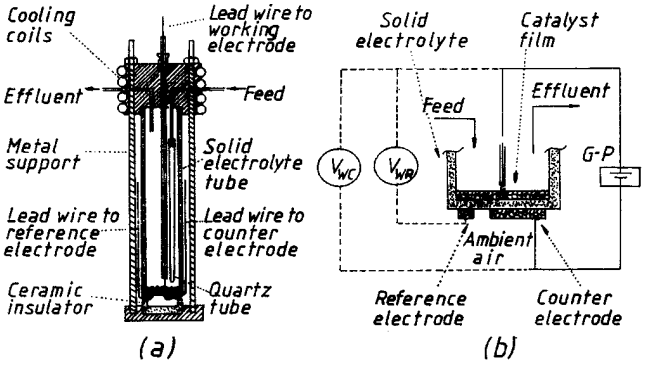

FIG. 1. Zirconia catalytic reactor, (a) Schematic of the reactor, (b) Catalyst and auxiliary electrode configuration.

ing in air by first raising the temperature at a rate 5°C/min to 400°C, maintaining it at 400°C for 2 h and then raising it at a rate 5°C/min to 700°C and maintaining it at 700°C for 2 h. Porous Ag catalyst films deposited in this mode have thickness on the order of 5–10 μm and have been shown by AES (53) to contain no detectable metal impurities. Typical scanning electron micrographs of such films have been shown previously (22, 26).

Three silver catalyst films were studied in the present investigation and all showed the same qualitative kinetic behavior. Their surface area, expressed in surface mol of O (Table 1) was determined by measuring their reactive oxygen uptake at 400°C via titration with ethylene as described previously (22, 28, 53, 54). In this isothermal method the Ag catalyst film is first exposed to air at 400°C for a time t_{O_2} (10–15 min) and the reactor is then purged with a high flow (~400 cm^3 STP/min) of ultrapure He for a time t_{He} sufficiently long (>50 s) to remove gaseous oxygen (54). Subsequently a certified standard of C_2H_4 in He is supplied at the same flow rate and the product CO_2 peak detected by the IR analyzer is integrated to provide the amount of oxygen n_O (t_{He}) present on the catalyst surface at t_{He}. A second peak provides a measure of the subsurface oxygen (54). By varying t_{He} one can study the kinetics of oxygen desorption (54). By extrapolating n_O (t_{He}) to $t_{He} = 0$ one obtains the maximum reactive oxygen uptake N (Table 1). The error introduced due to the parallel formation of ethylene oxide can be corrected (54) but is small (<5%) due to the low (<30%) selectivity to ethylene oxide at 400°C and the low (1 to 6) ratio of oxygen atoms needed for epoxidation and complete oxidation, respectively.

TABLE 1

Catalyst film	Reactive oxygen uptake of catalyst film (N/mol O)
ZR1	6.0×10^{-6}
ZR2	1.6×10^{-5}
ZR3	2.5×10^{-6}

Silver counter and reference electrodes were deposited by the same procedure on the air-exposed side of the bottom of the YSZ tube. A HEKA PG 284 galvanostat–potentiostat was used to apply constant currents I between the catalyst and the counter electrode (galvanostatic operation) or constant potentials V_{WR} between the catalyst (W, working electrode) and the reference (R) electrode (potentiostatic operation), as described in detail elsewhere (26).

RESULTS

Transients. Figures 2a and 2b show typical galvanostatic transients, i.e., they depict the response of the rates of ethylene oxide and CO_2 formation (expressed in mol C_2H_4/s) and of the catalyst potential V_{WR} to a step change in applied positive current I which corresponds to a rate $I/2F$ of O^{2-} supply to the catalyst.

Figure 2a was obtained with the Ag catalyst film labeled ZR1 (Table 1, reactive oxygen catalyst uptake $N = 6.0 \times 10^{-6}$ mol O). At the start of the experiment the circuit is open ($I = 0$) and the rates of epoxidation and deep oxidation are $r_{o,C_2H_4O} = 9.3 \times 10^{-10}$ mol C_2H_4/s and $r_{o,CO_2} = 6.0 \times 10^{-10}$ mol C_2H_4/s, respectively. The corresponding selectivity to ethylene oxide is thus $S_o = 60\%$.

At $t = 0$ the galvanostat is used to apply a constant current $I = 100$ μA between the counter electrode and the catalyst with a concomitant rate of oxygen transfer to the catalyst $I/2F = 5.2 \times 10^{-10}$ mol O/s. Both catalytic rates $r_{C_2H_4O}$ and r_{CO_2} start increasing and within 80 min stabilize to their new steady-state values which are 32.7×10^{-10} and 30.0×10^{-10} mol C_2H_4/s for the epoxidation and deep oxidation reaction, respectively, i.e., 250 and 400% higher than their open circuit values. The selectivity to epoxide drops to 52%. The corresponding increase Δr_O in the total rate of atomic oxygen consumption ($\Delta r_O = \Delta r_{C_2H_4O} + 6\Delta r_{CO_2}$) is 16.7×10^{-9} mol O/s. This is 32 times larger than $I/2F$, i.e., $\Lambda = 32$ and thus the system exhibits NEMCA behavior. Each O^{2-} supplied to the catalyst causes, on the average, 32 additional chemisorbed oxygen atoms to react.

As shown on the same figure the rate transients are accompanied by a transient in catalyst potential from $V^o_{WR} = -200$ mV for $I = 0$ to 150 mV for $I = 100$ μA. The observed changes in catalytic rates and V_{WR} are quite reversible. Upon current interruption $r_{C_2H_4O}$, r_{CO_2}, and V_{WR} tend to relax to their open circuit values. The V_{WR} transient is much faster than the rate transients for this system as also observed in earlier work (26). The origin of this type of behavior has been discussed recently (22, 26).

Similar transient behavior is observed in the case of catalyst film ZR2 ($N = 1.6 \times 10^{-5}$) upon imposition of a positive current $I = 50$ μA (Fig. 2b). In this case the steady-state rate increases for the epoxidation and deep oxidation are

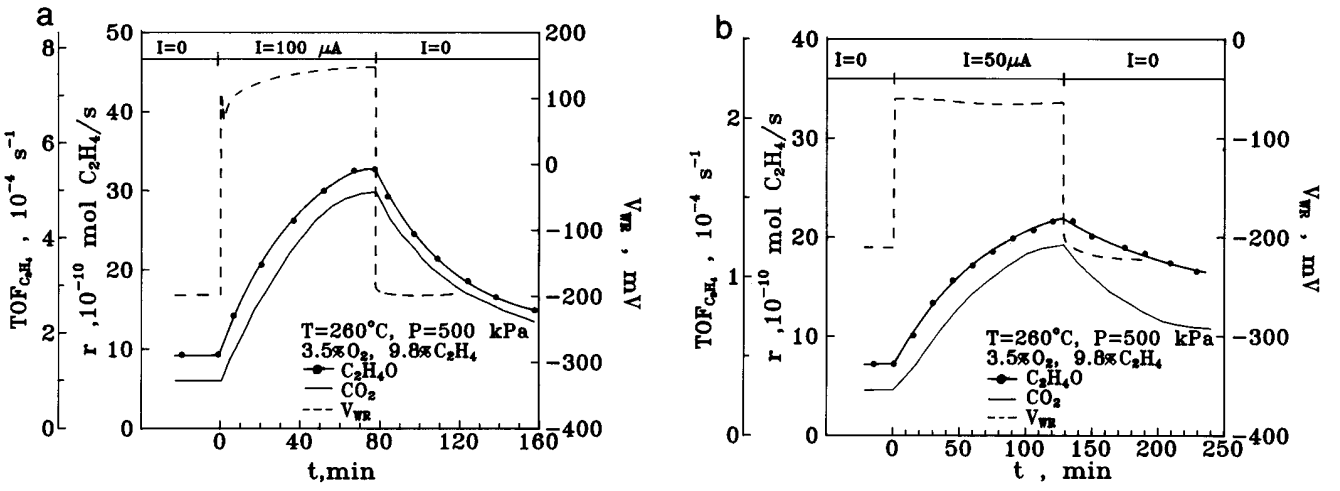

FIG. 2. Rate and catalyst potential response to step changes in applied positive current; (a) catalyst ZR1, $I = +100\ \mu$A; (b) catalyst ZR2, $I = +50\ \mu$A. Rates are also expressed as turnover frequency ($TOF_{C_2H_4}$), i.e., molecules of ethylene reacting per surface oxygen site per second. See text for discussion.

205 and 320%, respectively, with a concomitant decrease in selectivity to epoxide from 61 to 53% and a Λ value equal to 39.

Relaxation time constants and the coverage of the promoting $O^{\delta-}$ species. *In situ* XPS investigations of Ag (55–58) and Pt (42) films on YSZ subject to O^{2-} pumping have confirmed the proposition (19, 20, 22–24, 59) the NEMCA is due to an electrochemically controlled migration (backspillover) of oxide ions $O^{\delta-}$ from the YSZ solid electrolyte onto the catalyst surface. The same conclusion has been reached recently via *in situ* surface enhanced Raman spectroscopic (SERS) investigation of Pt films deposited on YSZ (60). These oxygen species, with an O1s binding energy of 528.8–529 eV (42), are accompanied by their compensating (screening) charge $M^{\delta+}$ in the metal, thus forming backspillover dipoles $O^{\delta-}$–$M^{\delta+}$ (22, 42, 59). These backspillover oxygen species are less reactive than normally chemisorbed oxygen (42) and act as promoters by increasing the catalyst work function and affecting the binding strength of chemisorbed reactants and intermediates (20, 22, 43–45, 59, 61). Consequently, the catalytic rate relaxation curves (Figs. 2a and 2b) upon current imposition and interruption convey useful information about the coverage of the promoting $O^{\delta-}$–$M^{\delta+}$ species and also about the kinetics of the reaction(s) which scavenge the promoting species from the catalyst surface, e.g., desorption or reaction with ethylene.

Current interruption. It has been shown (29, 37, 52) that the coverage $\theta_{O^{\delta-}}$ of the promoting oxide species after current interruption is given by

$$\theta_{O^{\delta-}}(t) = -\frac{I \ln(r(t)/r^*)}{2FN(d \ln(r(t)/r^*)/dt)}, \qquad [5]$$

where $r(t)$ is the catalytic rate at any time t after current interruption ($t = 0, r = r^*$), I is the previously applied current, and N is the total catalyst surface area in mol of metal.

Figure 3 shows the time evolution of $\theta_{O^{\delta-}}$ after current interruption for the cases of the two transients shown in Fig. 2. As shown on Fig. 3 the maximum $\theta_{O^{\delta-}}$ values are 0.45 and 0.2, respectively, for the transients of Figs. 2a and 2b. These are also the steady-state coverage values before current interruption. One can use Fig. 3 to compute $d\theta_{O^{\delta-}}/dt$ as a function of $d\theta_{O^{\delta-}}/dt$ and thus obtain Fig. 4, which depicts the kinetics of the reaction which scavenges $O^{\delta-}$ from the catalyst surface. As shown in Fig. 4 the rate of $O^{\delta-}$ removal increases linearly with backspillover oxygen coverage above a $\theta_{O^{\delta-}}$ value of 0.1 with a rate constant $k_s = 1.6 \times 10^{-4}\ s^{-1}$ for both catalyst films.

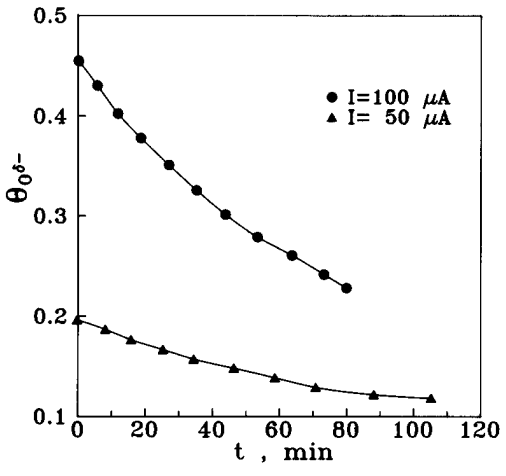

FIG. 3. Time evolution of the coverage $\theta_{O^{\delta-}}$ of the promoting oxide species after current interruption for the cases of the two transients shown in Fig. 2; see text for discussion.

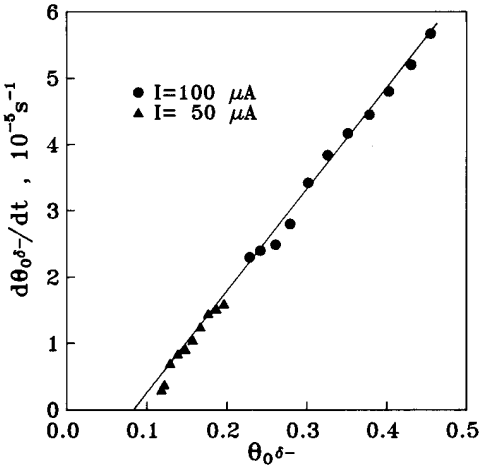

FIG. 4. Dependence of the scavenging reaction rate $d\theta_{O^{\delta-}}/dt$ on the coverage, $\theta_{O^{\delta-}}$, of the promoting $O^{\delta-}$ species after current interruption for the cases of the two transients shown in Fig. 3.

The low value of k_s, which is approximately Λ times smaller than the turnover frequency of normal chemisorbed oxygen (Ref. 37 and Fig. 2) explains the slow return of the catalytic rates to their open-circuit values after current interruption. It also explains why $O^{\delta-}$ can act as a promoter, since its lifetime on the surface is of the order of Λ times longer than that of normally chemisorbed atomic oxygen (37).

Current imposition. Previous NEMCA studies utilizing O^{2-} conductors as the solid electrolyte have established that the order of magnitude of the rate relaxation time constant τ (22, 23) upon current imposition during galvanostatic transients is of the order of $2FN/I$ (22, 23). This is also the case here as can be seen from the transients of Fig. 2 where $2FN/I$ is 193 and 103 min, respectively, for Figs. 2a and 2b. It is interesting to notice that the agreement tends to become closer if one compares τ with $2FN\theta_{O^{\delta-},max}/I$, where $\theta_{O^{\delta-},max}$ are the $O^{\delta-}$ coverages computed from the transients upon current interruption. This parameter takes the values 87 and 20 min in Figs. 2a and 2b, respectively. This corroborates further the validity of Eq. [5] and the fact that NEMCA on Ag is, as in the case of Pt (42) due to oxide ion migration. The latter also follows directly from the XPS spectra of Arakawa *et al.* (55, 56).

Steady-state effect of current. Figures 5a and 5b show the steady-state effect of current on the total rate of ethylene oxidation, i.e., both epoxidation and complete oxidation, expressed in mol O/s. Ethylene epoxidation is an electrophobic reaction (22, 26, 47, 48), i.e.,

$$\frac{\partial r}{\partial I} > 0; \quad \frac{\partial r}{\partial V_{WR}} > 0; \quad \frac{\partial r}{\partial (e\Phi)} > 0. \qquad [6]$$

The Faradaic efficiency Λ ($= \Delta r(I/2F)$) is typically of the order of 100; i.e., each O^{2-} supplied to the catalyst causes, on the average, 100 chemisorbed oxygen atoms to react with ethylene forming ethylene oxide and CO_2.

The measured Λ values are in good agreement with the parameter $2Fr_o/I_0$ (Fig. 6) and with those measured in previous atmospheric pressure NEMCA studies of C_2H_4 oxidation on Ag (26, 47).

Effect of catalyst potential V_{WR} and work function $e\Phi$. Figure 7a shows the effect of varying catalyst potential V_{WR} and corresponding (20, 22, 59) work function change $\Delta(e\Phi)$ on the rates of formation of C_2H_4O, CO_2 and CH_3CHO, expressed in mol C_2H_4/s and also in turnover frequency (TOF), i.e., molecules ethylene reacting per surface oxygen site per second.

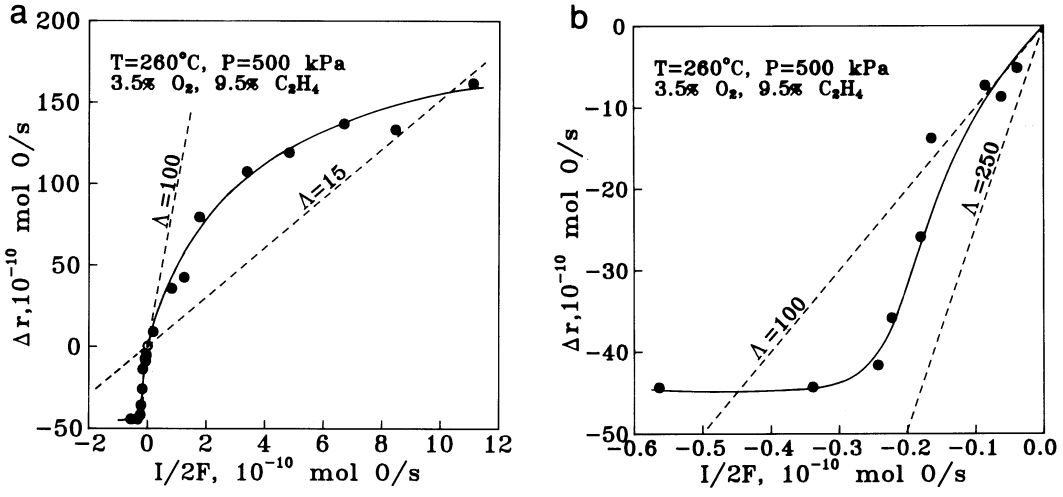

FIG. 5. Steady-state effect applied current on the total rate of ethylene oxidation, expressed in mol O/s. Dashed lines are constant enhancement factor Λ lines. Open symbols correspond to open circuit conditions: catalyst ZR1 (a) $I > 0$ and $I < 0$; (b) $I < 0$ (detailed view).

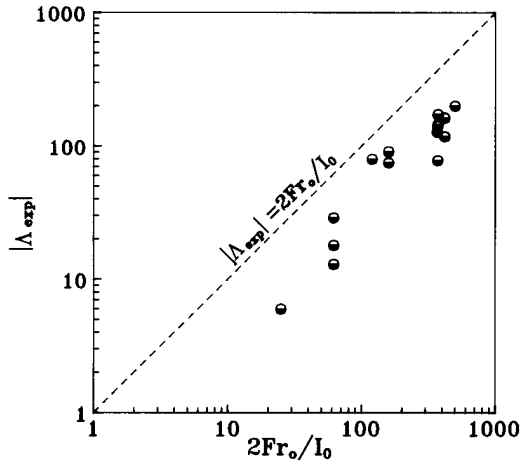

FIG. 6. Comparison of the parameter $2Fr_o/I_0$ values with the measured enhancement factor Λ values for the total rate of ethylene oxidation; see text for discussion.

The top axis in the figure is based on the equality

$$\Delta(e\Phi) = e\Delta V_{WR}, \qquad [7]$$

established both theoretically (22–24) and experimentally via *in situ* Kelvin probe measurements (vibrating capacitor method) (20, 59).

As shown in Fig. 7, both the epoxidation and the complete oxidation rates increase by a factor of 230 as the work function $e\Phi$ is increased by 0.6 eV. The rate enhancement ratio ρ ($= r/r_o$) varies approximately between 0.02 and 4.6, i.e., by a factor of 230. This is the largest variation of ρ with $e\Phi$ observed in NEMCA studies utilizing O^{2-} conductors.

A rule which has emerged from previous NEMCA studies is that

$$\ln(r/r_o) = \alpha\Delta(e\Phi)/k_bT, \qquad [8]$$

where the NEMCA coefficient α is positive for electrophobic reactions, such as ethylene epoxidation and negative for electrophilic reactions. As shown on Fig. 7a the rate dependence on $e\Phi$ is here more complex, indicating that the NEMCA coefficients $\alpha_{C_2H_4O}$ and α_{CO_2} vary with catalyst potential.

It is worth noting the qualitative similarity in the work function dependence of the rates of epoxidation and complete oxidation. This similarity corroborates the existence of a common adsorbed intermediate, i.e., atomic oxygen, for the production of both C_2H_4O and CO_2.

Interestingly, for $V_{WR} < 0.5$ V acetaldehyde is also produced in measurable amounts. It most likely originates from the isomerization of ethylene oxide, as discussed below.

Figure 7b is based on the data of Fig. 7a and presents the effect of V_{WR} and $\Delta(e\Phi)$ on the selectivity to ethylene oxide and acetaldehyde. The selectivity to ethylene oxide is up to 62% and exhibits two well defined maxima. Figure 7b also shows the effect of V_{WR} and $\Delta(e\Phi)$ on the NEMCA coefficients α of Eq. [8] for the epoxidation (solid line) and complete oxidation (dashed line) reactions computed via Eq. [8] from the slopes of the curves of Fig. 7a, i.e., from

$$\alpha_{C_2H_4O} = \frac{RT}{F}\cdot\frac{d\ln r_{C_2H_4O}}{dV_{WR}}; \quad \alpha_{CO_2} = \frac{RT}{F}\cdot\frac{d\ln r_{CO_2}}{dV_{WR}}, \qquad [8a]$$

where $r_{C_2H_4O}$ and r_{CO_2} are the rates of epoxidation and complete oxidation, respectively. It is remarkable that the two

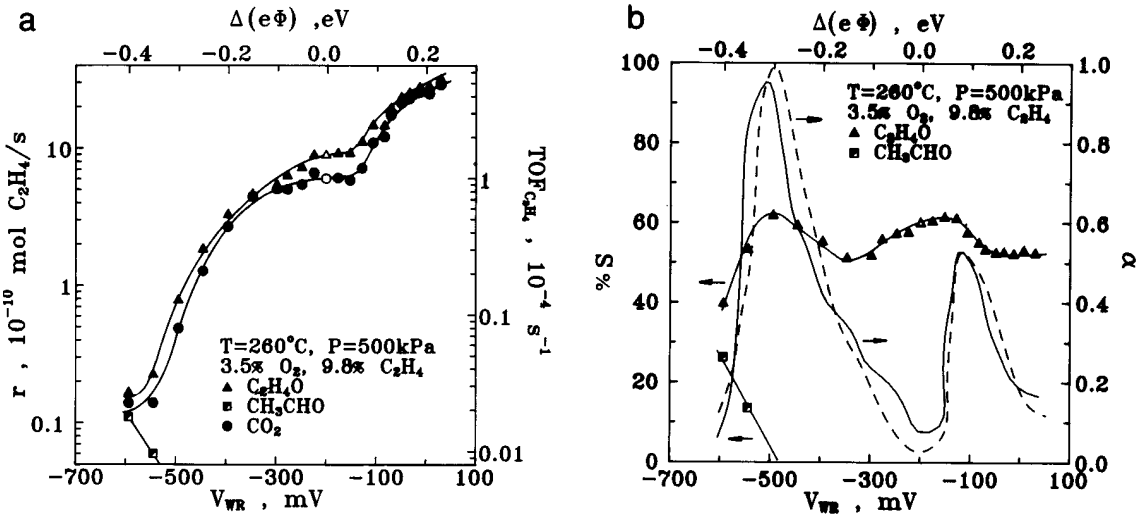

FIG. 7. (a) Effect of catalyst potential and corresponding work function change on the rates and corresponding turnover frequencies of formation (molecules C_2H_4 reacting per surface O site per sec) of ethylene oxide, CO_2, and acetaldehyde for $P_{C_2H_4}/P_{O_2} = 2.8$; open symbols correspond to open-circuit ($I = 0$) conditions; catalyst, ZR1. (b) Effect of catalyst potential and corresponding work function change on the NEMCA coefficient $\alpha_{C_2H_4O}$ (solid line), α_{CO_2} (dashed line), and on the selectivity to ethylene oxide and acetaldehyde for $P_{C_2H_4}/P_{O_2} = 2.8$; conditions as in Fig. 7a.

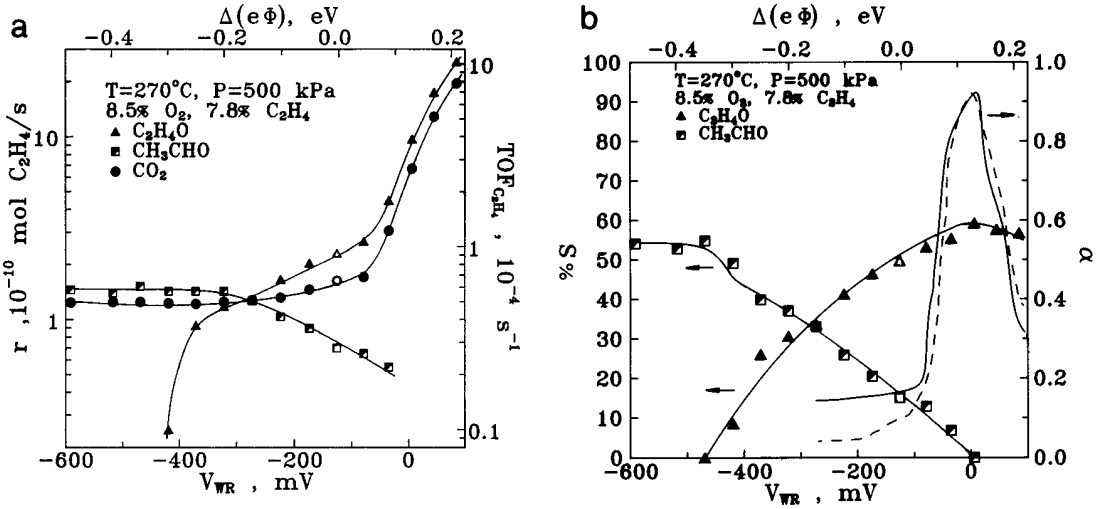

FIG. 8. (a) Effect of catalyst potential and corresponding work function change on the rates and corresponding turnover frequencies of formation of ethylene oxide, CO_2, and acetaldehyde for $P_{C_2H_4}/P_{O_2} = 0.92$; open symbols correspond to open-circuit ($I = 0$) conditions; catalyst, ZR3. (b) Effect of catalyst potential and corresponding work function change on the NEMCA coefficients $\alpha_{C_2H_4O}$ (solid line), α_{CO_2} (dashed line), and on the selectivity to ethylene oxide and acetaldehyde for $P_{C_2H_4}/P_{O_2} = 0.92$.

selectivity maxima occur at the same potential values where the NEMCA coefficients α are also maximized (Fig. 7b).

The selectivity to acetaldehyde increases sharply with decreasing V_{WR} (Fig. 7b). It is worth noting that acetaldehyde production is not observed under the same operating conditions when using β''–Al_2O_3 as the solid electrolyte (49). This may be due to the suppression in acetaldehyde formation with the addition of alkalis reported by Lambert and co-workers (7).

As shown in Figs. 8a and 8b, acetaldehyde production is significantly enhanced at higher oxygen to ethylene ratios (1.1 : 1). Here the open-circuit selectivity to ethylene oxide and acetaldehyde is 50 and 16%, respectively. Increasing $e\Phi$ causes an increase in ethylene oxide selectivity up to 59%, while the selectivity to acetaldehyde vanishes. Decreasing $e\Phi$ causes a substantial increase in the selectivity to acetaldehyde up to 55% while the selectivity to ethylene oxide vanishes. Thus by varying $e\Phi$ by 0.5 eV one obtains a dramatic selectivity change as the catalyst shifts from ethylene oxide production to acetaldehyde production (Fig. 8b).

The dependence of the rates of formation of ethylene oxide and CO_2 on V_{WR} (Fig. 8a) bears several similarities with that obtained for low O_2 to ethylene ratios (Fig. 7a). The selectivity to ethylene oxide is again maximized in the V_{WR} region where the NEMCA coefficients α are also maximized. At this maximum both $\alpha_{C_2H_4O}$ and α_{CO_2} have values near unity (Fig. 8b). It is worth noting that the low $e\Phi$ selectivity maximum is missing here due to the formation of acetaldehyde.

Ethylene isomerization. In order to examine whether acetaldehyde is a primary partial oxidation product or it is produced from ethylene oxide isomerization, a series of kinetic experiments was carried out with only ethylene oxide present in the feed (0.1% ethylene oxide diluted in He). The key results are shown in Figs. 9a and 9b, which depict the effect of current and catalyst potential on the rate of isomerization of ethylene oxide to acetaldehyde which was the only product detected. As shown in these figures, ethylene oxide isomerization to acetaldehyde exhibits a strong electrophilic NEMCA effect with Λ values as low as -280 (Fig. 9a) with ρ varying between 0.5 and 2.6 as the catalyst potential is decreased from 0 to -2 V. These results are consistent with the observed pronounced increase in the rate of acetaldehyde production for low catalyst potentials (Fig. 7 and 8) and can be attributed to the weakening of the chemisorptive bond of ethylene oxide, which is a strong electron donor, with decreasing catalyst work function.

Effect of chlorinated hydrocarbon "moderators." Figure 10 shows the effect of the gas-phase addition of various levels of 1,2-$C_2H_4Cl_2$ on the selectivity to ethylene oxide as a function of catalyst potential under *reducing* gas-phase conditions. The selectivity to ethylene oxide varies between 53 and 78% and its dependence on $P_{C_2H_4Cl_2}$ is rather complex with the appearance of one maximum at 0.3 ppm $C_2H_4Cl_2$, for all potentials, and of a second range of small selectivity increase at high $P_{C_2H_4Cl_2}$ values observed only for low catalyst potentials. This is reminiscent of the selectivity dependence on V_{WR} under the same gas-phase composition which exhibits two maxima (Fig. 7b).

The corresponding effect of $P_{C_2H_4Cl_2}$ and catalyst potential on the rates of formation of C_2H_4O and CO_2 under reducing conditions is shown in Figs. 11a and 11b. For highly negative overpotentials, increasing $P_{C_2H_4Cl_2}$ enhances both rates, while for highly positive overpotentials increasing

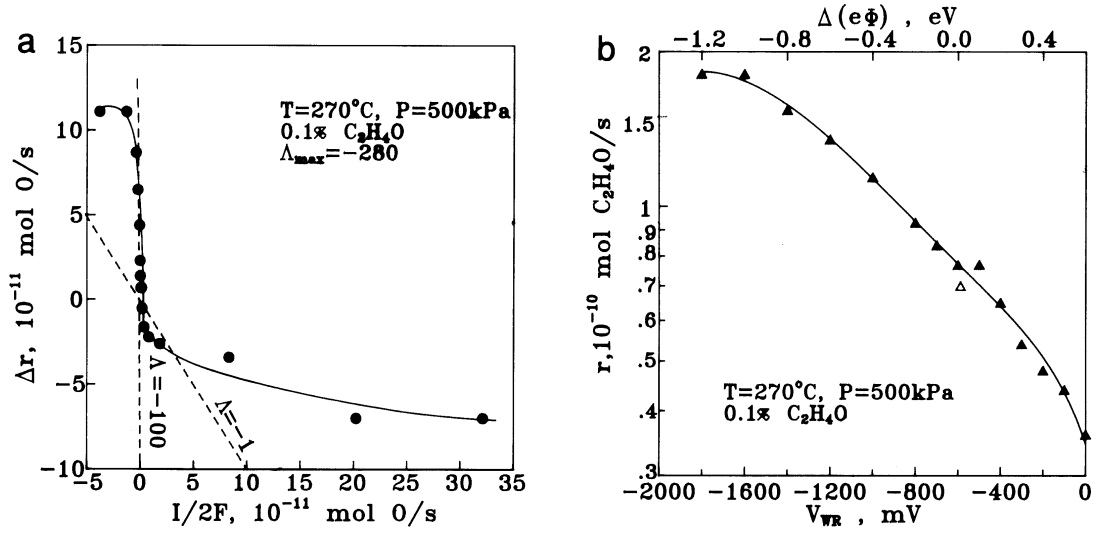

FIG. 9. (a) Effect of applied current on the change in the rate of ethylene oxide isomerization to acetaldehyde; dashed lines are constant enhancement factor (faradaic efficiency) Λ lines; catalyst, ZR3. (b) Effect of catalyst potential on the rate of isomerization of ethylene oxide to acetaldehyde; conditions as in (a).

$P_{C_2H_4Cl_2}$ decreases both rates. For intermediate potentials the rates go through a maximum at $P_{C_2H_4Cl_2} = 0.6$ ppm.

Figures 12a and 12b show the effect of the gas-phase addition of various levels of 1,2-$C_2H_4Cl_2$ on the selectivity to ethylene oxide (Fig. 12a) and acetaldehyde (Fig. 12b) as a function of catalyst potential V_{WR} and work function $e\Phi$ under "*oxidizing*" gas-phase conditions. Increasing dichloroethane concentration causes a pronounced decrease in the selectivity to acetaldehyde (Fig. 12b) and a concomitant pronounced increase in the selectivity to ethylene oxide (Fig. 12a). Thus at $V_{WR} = -0.5$ V the selectivity to ethylene oxide increases from 0 to 58% by the addition of 2 ppm 1,2-C_2H_4Cl. For $V_{WR} = 0.0$ V the selectivity increases from 59 to 73%.

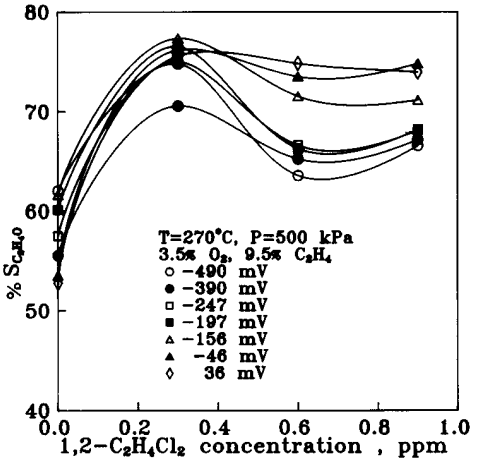

FIG. 10. Effect of 1,2-$C_2H_4Cl_2$ gas phase concentration and catalyst potential V_{WR} on the selectivity to ethylene oxide: catalyst, ZR1; $P_{C_2H_4}/P_{O_2} = 2.7$; open circuit potential at zero dichloroethane concentration $V^o_{WR} = -197$ mV.

By comparing Fig. 7b with Fig. 10 (reducing conditions) and Fig. 8b with Fig. 12a ("oxidizing" conditions) one observes that Cl addition and variation in V_{WR} and $e\Phi$ produce qualitatively the same effects in ethylene oxide selectivity.

In order to investigate further the role of dichloroethane, a series of open-circuit kinetic experiments was carried out where the rate dependence on P_{O_2} and $P_{C_2H_4}$ was studied in absence and in presence of 1,2-$C_2H_4Cl_2$. Typical examples are presented in Figs. 13a and 13b. As shown in Fig. 13a the rates of epoxidation and deep oxidation follow a Langmuir-type dependence on $P_{C_2H_4}$. Addition of dichloroethane suppresses both rates and decreases the $P_{C_2H_4}$ value necessary to reach rate saturation. This strongly indicates enhanced binding of C_2H_4 on the catalyst surface, i.e., the same effect caused by increasing $e\Phi$.

Figure 13b shows the rate dependence on P_{O_2} without and with dichloroethane. Without dichloroethane both rates are near second order in oxygen. Addition of 1,2-$C_2H_4Cl_2$ suppresses both rates which become near first order in P_{O_2} and enhances the selectivity to ethylene oxide.

Electrokinetic behavior. Figure 14 presents typical current–overpotential curves under oxidizing conditions at various levels of dichloroethane. The overpotential η is defined as the deviation of the catalyst potential V_{WR} from its open-circuit ($I = 0$) V^o_{WR} value; i.e., $\eta = V_{WR} - V^o_{WR}$ (22, 26). Cathodic operation ($\eta < 0$) leads to limiting current behavior in agreement with previous atmospheric pressure studies of Ag/YSZ (62). As shown in Fig. 14 the cathodic limiting current goes through a maximum with increasing $P_{C_2H_4C_2}$ at $P_{C_2H_4Cl_2} = 0.6$ ppm. This behavior parallels the

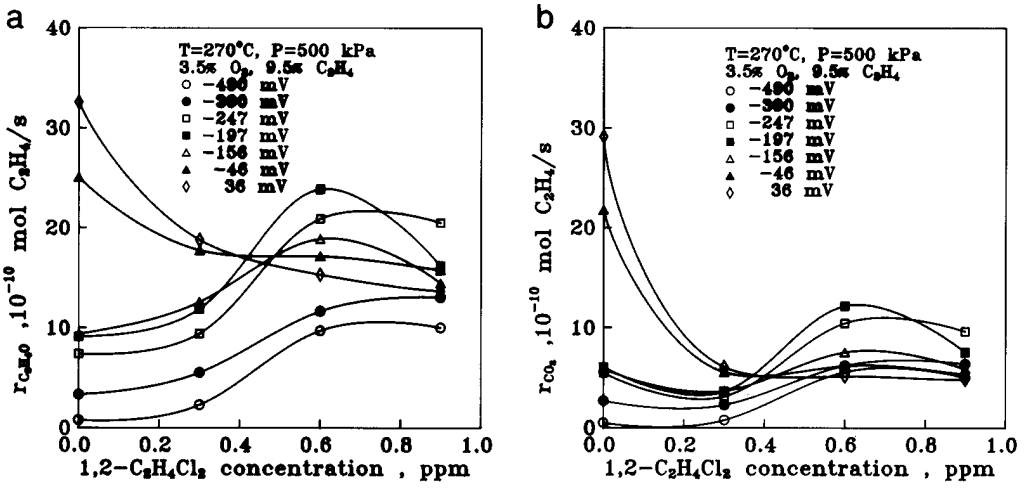

FIG. 11. Effect of 1,2-$C_2H_4Cl_2$ gas phase concentration and catalyst potential V_{WR} on the rate of formation of ethylene oxide (a) and CO_2 (b); conditions as in Fig. 10.

catalytic rates dependence on $P_{C_2H_4Cl_2}$ (Figs. 11a and 11b). The data of Fig. 14 were fitted to a generalized form of the Butler–Volmer equation (46, 63, 64),

$$I = \frac{\exp(\alpha_a F\eta/RT) - \exp(-\alpha_c F\eta/RT)}{(1/I_0) + (1/I_{L,c})\exp(\alpha_c F\eta/RT)}, \qquad [9]$$

where α_a and α_c are the anodic and cathodic transfer coefficients, respectively, I_0 is the exchange current density, and $I_{L,c}$ is the cathodic limiting current, to obtain the I_0 and $I_{L,c}$ results shown on Fig. 15. Both I_0 and $I_{L,c}$ go through a maximum at $P_{C_2H_4Cl} = 0.6$ ppm, i.e., at the same dichloroethane concentration which maximizes the rates of epoxidation and deep oxidation (Figs. 11a and 11b).

It is known (26, 54, 65) that oxygen dissolution and diffusion in the Ag catalyst affects the electrokinetic behavior of this system. The observed low limiting currents for cathodic operation are due to enhanced binding of oxygen on the Ag catalyst with negative potentials (26, 65).

DISCUSSION

The present results show that doped zirconia solid electrolytes can be used as active catalyst supports to significantly and reversibly affect the catalytic properties of Ag for the epoxidation and deep oxidation of ethylene by utilizing the NEMCA effect. In comparison to earlier, atmospheric pressure, studies of the NEMCA effect in ethylene epoxidation, the present work has focused on conditions similar to those employed in industrial practice, i.e., high operating pressure (500 kPa), low temperatures (260°C), fuel rich conditions, and use of chlorinated hydrocarbon moderators.

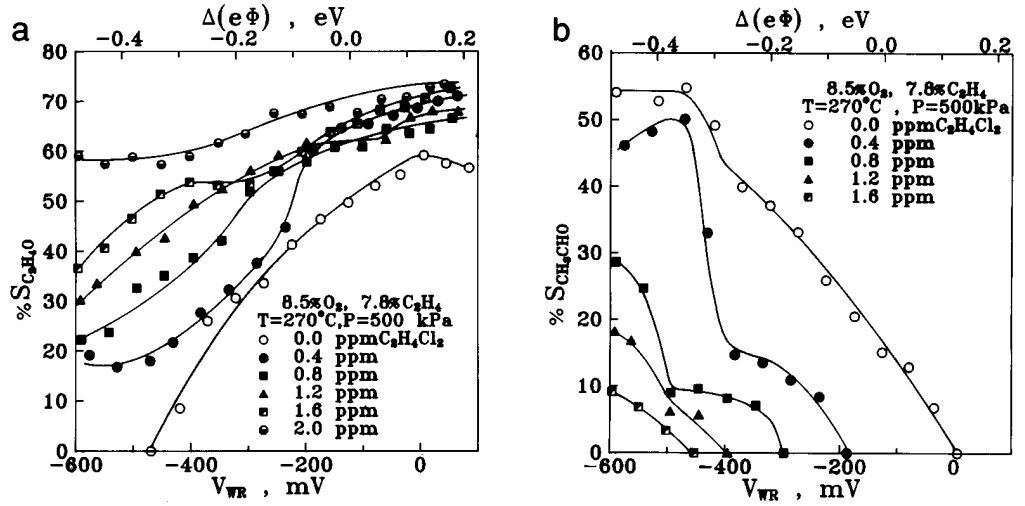

FIG. 12. Effect of the gas-phase addition of various levels of 1,2-$C_2H_4Cl_2$ on the selectivity to ethylene oxide (a) and acetaldehyde (b) as a function of catalyst potential V_{WR} and work function. Catalyst, ZR3; $P_{C_2H_4}/P_{O_2} = 0.92$.

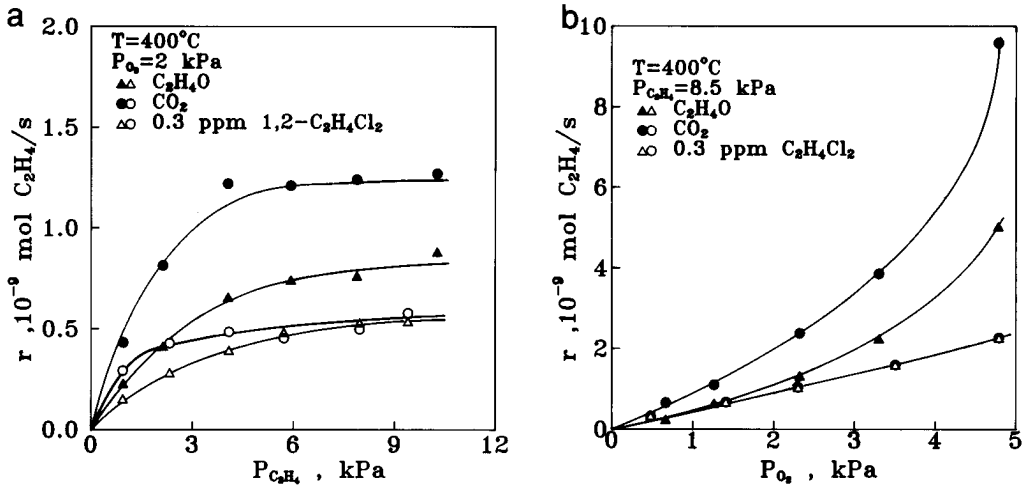

FIG. 13. Dependence of the rates of epoxidation and deep oxidation on the gas phase concentration of 1,2-$C_2H_4Cl_2$ and on $P_{C_2H_4}$ (a) and P_{O_2} (b); catalyst, ZR4.

Under these conditions it is found that the effect of potential, or equivalently (20, 22, 59) catalyst work function, is very pronounced, as the catalytic activity is altered by a factor up to 230 with enhancement factor Λ values up to 200.

As in previous NEMCA studies the observed Λ values both for the epoxidation and deep oxidation reaction are close to the ones predicted by

$$|\Lambda| = 2Fr_o/I_0, \qquad [10]$$

where r_o is the total open circuit catalytic rate and I_0 is the exchange current density (Fig. 6).

The selectivity to C_2H_4O is also altered significantly by changing the catalyst potential and reaches a maximum value of 78% (Fig. 10). For low catalyst work function $e\Phi$ values the selectivity to acetaldehyde is up to 55% (Fig. 12b).

The observed behavior is complex and defies a rigorous quantitative description. All the observed features can, however, be rationalized qualitatively by taking into account the effect of changing $e\Phi$ and concomitant change in the coverage of backspillover oxide ion species with positive $\Delta(e\Phi)$ on the strength of the chemisorptive bonds of the reactive surface species, i.e., of covalently bonded ethylene and atomic oxygen (22, 43), in conjunction with the prevailing ideas about the mechanism of the ethylene epoxidation system (4). It is well known that several forms of oxygen can exist on Ag surfaces. These include (I) molecularly adsorbed oxygen, which is rather inactive and has been shown by Lambert and co-workers to behave as a "spectator" species (5, 6); (II) atomic oxygen, which has

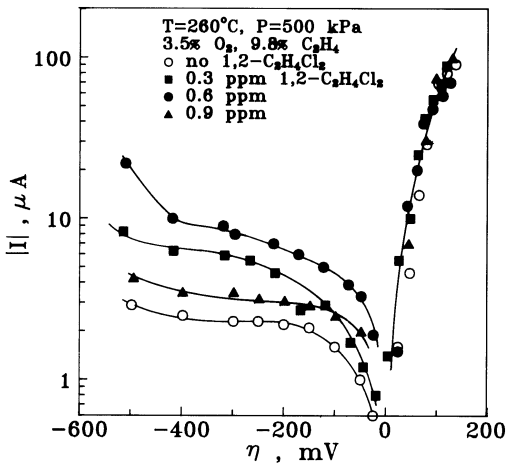

FIG. 14. Typical current–overpotential curves at various levels of gaseous 1,2-$C_2H_4Cl_2$ concentrations; catalyst, ZR1; $P_{C_2H_4}/P_{O_2} = 2.8$.

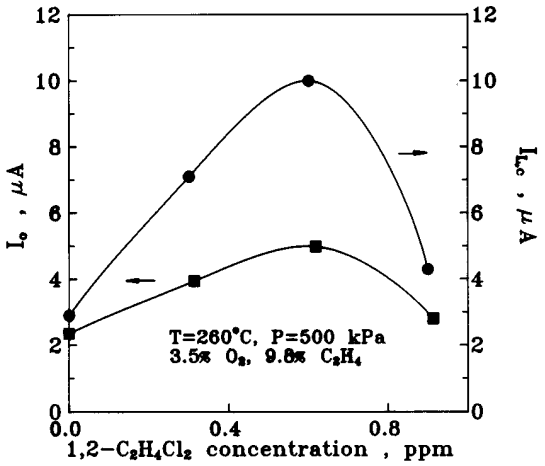

FIG. 15. Dependence of the exchange current I_0 and of the cathodic limiting current $I_{L,c}$ on 1,2-$C_2H_4Cl_2$ concentration; conditions as in Fig. 14.

been shown to be the reactive oxygen species for both ethylene epoxidation and deep oxidation (4–10); and (III) subsurface oxygen, which is necessary for obtaining high selectivity to epoxide, although it does not directly participate in catalytic events (4, 8, 66). The presence of subsurface oxygen causes a weakening of the chemisorptive bond strength of adsorbed atomic oxygen via withdrawal of electrons from the silver sites, thus favoring the creation of weakly bound, electrophilic oxygen atoms which produce epoxide (4). Strongly bound, bridging, oxygen atoms coordinated to Ag ions of low charge react preferentially with the hydrogen atoms of the ethylene molecule, with concomitant C–H bond rupture and CO_2 formation (4, 18).

In addition to the above forms of oxygen one must also take into account in the present case the presence of backspillover oxide ions $O^{\delta-}$ which migrate onto the catalyst surface with positive currents, i.e., when $\Delta(e\Phi > 0)$ as shown by XPS (55, 56, 58). These species are Λ ($\sim$100) times less reactive than atomic oxygen and thus act as promoters (22, 42–45).

Ethylene adsorption on Ag is weak (4, 67–70) but is enhanced in the presence of preadsorbed oxygen, which creates on the silver surface positively charged sites which are necessary for ethylene adsorption (2, 4, 12). Thus C_2H_4 is adsorbed on such sites with the C–C bond parallel to the surface and with transfer of electron density from the double bond to the surface (4, 12, 68, 69).

Types of atomic oxygen responsible for epoxidation and deep oxidation. As previously noted two types of dissociatively chemisorbed oxygen are believed to play an important role in the epoxidation and complete oxidation reactions (4–13); as shown in Fig. 16:

(a) weakly bound, electrophilic adsorbed oxygen which reacts preferentially with the π-electrons of adsorbed ethylene thus producing epoxide (4, 5, 11–13);
(b) strongly bound, bridging oxygen atoms coordinated to Ag ions of low charge which attack preferentially the H atoms of adsorbed ethylene with a concomitant C–H bond rupture and CO_2 formation (4, 5, 11–13).

For brevity in the following discussion we refer to these two types of adsorbed oxygen as α- (or electrophilic) oxygen and β- (or ionic) oxygen, respectively. As originally shown by Grant and Lambert (5) and as also supported by the present work, as discussed below, these two states of adsorbed oxygen must be considered as two different extreme conformations of the same atomic oxygen species and not as two intrinsically distinct forms which coexist on the surface. There appears to be only one type of atomic oxygen leading both to epoxidation and complete oxidation. Depending on the operating conditions, however, this atomic oxygen can behave as predominantly electrophilic or ionic.

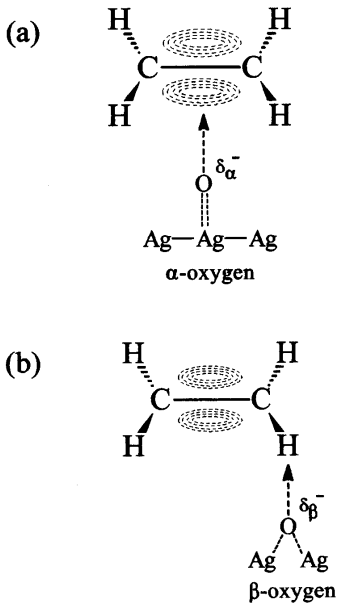

FIG. 16. Schematic of the two extreme conformations of adsorbed atomic oxygen: covalently bonded electrophilic oxygen (α-) and ionically bonded oxygen (β-).

In order to facilitate the discussion we first list the factors affecting the rates of epoxidation, complete oxidation, and acetaldehyde formation and the product selectivity. These include:

(a) the coverage of atomic oxygen, θ_O, and its predominantly α- or β-type character;
(b) the coverage of ethylene, $\theta_{C_2H_4}$, and ethylene oxide, $\theta_{C_2H_4O}$;
(c) the chemisorptive bond strength of atomic oxygen, ethylene, and ethylene oxide.

We then list the operating variables at our disposal in the present work. These include:

(a) the gas phase composition which affects θ_O, $\theta_{C_2H_4}$, and $\theta_{C_2H_4O}$, as well as the amount of subsurface oxygen (54);
(b) the catalyst potential V_{WR} and work function change $\Delta(e\Phi)$ which controls the coverage of spillover ions $\theta_{O^{\delta-}}$ and thus affects θ_O, $\theta_{C_2H_4}$, and $\theta_{C_2H_4O}$ and the corresponding binding strengths (22, 23, 43–45, 61) (V_{WR} also affects to a minor (Faradaic) extent the amount of subsurface oxygen (54). Since the latter is controlled both by gas phase composition and V_{WR} (54), no attempt will be made to separate its role and treat it as an independently controllable variable.);
(c) the chlorine coverage θ_{Cl} which is largely controlled by $P_{C_2H_4Cl_2}$ and which affects θ_O, $\theta_{C_2H_4}$, and $\theta_{C_2H_4O}$, and also the corresponding binding strengths.

Effect of operating variables on coverages and binding strengths. Table 2 shows the anticipated effect of the

TABLE 2

Expected Effect of the Operating Variables on Coverages θ_i and Binding Strengths E_i

	θ_O	$\theta_{O_\alpha}/\theta_{O_\beta}$	$\theta_{C_2H_4}$	$E_{O,\alpha}$	$E_{C_2H_4}$	r
$P_{O_2}/P_{C_2H_4}$ ↗	↗	↗	↘	↘	↗	↗ ↘
V_{WR}, $e\Phi$ ↗	↘	↗	↗	↘	↗	↗
Cl ↗	↘	↗	↗	↘	↗	↗ ↘

operating variables on the coverage and binding strengths of the adsorbed species relevant to epoxidation and complete oxidation. In the following discussion we justify these predictions and compare with experiment.

Effect of $e\Phi$ and gaseous composition. Increasing $e\Phi$ above its open-circuit value and thus providing $O^{\delta-}$ onto the catalyst surface is known (22, 59, 62) to weaken the binding strength of electron acceptor adsorbates, such as chemisorbed oxygen (54, 71) and to strengthen the chemisorptive bond strength of electron donor adsorbates, i.e., ethylene and ethylene oxide (4, 69, 70, 72). In the present case, increasing $e\Phi$ causes a strong enhancement in the rates by weakening the chemisorptive bond strength of atomic oxygen (Figs. 7a, 8a). This is also established by the observed pronounced decrease in activation energy of both reactions with increasing $e\Phi$, with slopes near -1 (26). In general increasing $e\Phi$ is also expected to enhance the selectivity to ethylene oxide by favoring the more weakly bonded electrophilic (α-) state of adsorbed oxygen (Figs. 7b, 8b) at least until the point is reached at very high $e\Phi$, where ethylene and also ethylene oxide which are electron donors (69, 70, 72), become more strongly bound on the surface and thus more susceptible to further oxidation (4, 26). These considerations can explain the observed increase in selectivity with increasing $e\Phi$ near the open-circuit conditions (Figs. 7b and 8b) and the appearance of the selectivity maximum at $\Delta(e\Phi) \approx 0.1$ eV.

Decreasing V_{WR} and $e\Phi$ below their open-circuit values via negative current application is known to cause a pronounced strengthening in the chemisorptive bond of oxygen (54) as also evidenced by the limiting current behavior under these conditions (Fig. 14). This is the cause of the pronounced decrease in the rates of epoxidation and complete oxidation (Figs. 7a and 8a) which is much more pronounced in reducing environments (Fig. 7a). Under these conditions a second maximum appears in the selectivity to ethylene oxide (Fig. 7b). It is possible that this maximum, also observed in atmospheric pressure ethylene epoxidation studies (26), is caused by preferential removal of ionic oxygen from the catalyst surface via the negatively applied current. This is corroborated by the concomitant increase in the NEMCA coefficients α (Fig. 7b), which is similar to the α behavior at the high $e\Phi$ ethylene oxide selectivity maximum.

An additional factor causing the second selectivity maximum may be the weakening in the chemisorptive bond of ethylene and also ethylene oxide which makes them less susceptible to complete oxidation. At very low $e\Phi$ values, however, the effect of strongly bound oxygen dominates and the selectivity to ethylene oxide decreases again (Fig. 7b).

It is worth nothing that the second ethylene oxide selectivity maximum is absent under "oxidizing" conditions (Fig. 8b) and instead there is a pronounced increase in the selectivity to acetaldehyde. This is consistent with the pronounced enhancement in the rate of ethylene oxide isomerization with decreasing $e\Phi$ (Fig. 9). The strong suppression in the rate of acetaldehyde production for high ethylene to oxygen ratios (Fig. 7) can be explained if ethylene and ethylene oxide compete for the same surface sites. If this is the case, the observed severe suppression in acetaldehyde production must be due to the low coverage of ethylene oxide under reducing conditions. Note that a low coverage of ethylene oxide does not imply a low rate of ethylene oxide production, as long as its desorption is not rate limiting. There is no evidence in the literature that desorption of ethylene oxide is rate limiting.

Effect of chlorine. The effect of chlorine addition on the selectivity to ethylene oxide (Figs. 10 and 12a) bears several interesting similarities with the effect of increasing V_{WR} and $e\Phi$ (Figs. 7b and 8b).

Thus under reducing conditions (Figs. 10 and 7b) both increasing Cl coverage and increasing $e\Phi$ cause the appearance of two ethylene oxide selectivity maxima, although in the former case the second maximum is not well defined.

Under oxidizing conditions (Figs. 12a and 8b) both increasing Cl coverage and increasing $e\Phi$ cause the appearance of only one selectivity maximum.

Furthermore, both Cl addition and increasing $e\Phi$ severely suppress the selectivity to acetaldehyde (Figs. 12b, 7a, and 8a).

There is, however, a certain synergy between these two parameters leading to ethylene oxide selectivities up to 78 and 73%, respectively, under reducing and oxidizing conditions (Figs. 10 and 12a). As evidenced by these figures neither dichloroethane addition nor NEMCA along suffices to attain these values.

Consequently, the main role of chlorine is to increase the catalyst work function and to favor the formation of weakly bonded electrophilic oxygen. On the other hand, it also blocks oxygen chemisorption sites.

This twofold role of chlorine is clearly manifested in Figs. 11a and 11b, which show the effect of Cl on the rates of epoxidation and complete oxidation at various fixed values of catalyst potential V_{WR} and $e\Phi$: When V_{WR} and $e\Phi$ are high and the Ag–O bond is thus already weak, the blocking

character of Cl dominates and both rates decrease monotonically with dichloroethane concentration (Fig. 11). For low V_{WR} and $e\Phi$ values, addition of Cl enhances both rates, via weakening of the Ag–O bond, until the point where the blocking character of Cl dominates and both rates go through a maximum is reached (Fig. 11). Interestingly, at this point both rates also go through a maximum with respect to V_{WR} as can be observed from Fig. 11. Beyond the maximum electrophilic behavior is thus obtained. This observation underlines again the similar roles of Cl addition and electrochemically induced work function increase.

NEMCA coefficients and selectivity. It is remarkable that the NEMCA coefficients $\alpha_{C_2H_4O}$ and α_{CO_2} are maximized at the same V_{WR} where the selectivity to ethylene oxide is also maximized (Figs. 7b and 8b). In general, the NEMCA coefficient α provides a measure of the charge which is transferred between the surface and the adsorbed species during the rate limiting step of catalytic reaction. An α value of unity implies that one electron is being transferred.

As shown in Figs. 7b and 8b the NEMCA coefficients $\alpha_{C_2H_4O}$ and α_{CO_2} vary between 0 and 1. As derived in the Appendix the selectivity to ethylene oxide S is related to $\alpha_{C_2H_4O}$ and α_{CO_2} via

$$\frac{dS}{S(1-S)} = \frac{F}{RT}(\alpha_{C_2H_4O} - \alpha_{CO_2})\, dV_{WR} \qquad [11]$$

and thus

$$\frac{S}{1-S} = \frac{S_o}{1-S_o}\exp\left(\frac{F}{RT}\int_{V_{WR}^o}^{V_{WR}} (\alpha_{C_2H_4O} - \alpha_{CO_2})\, dV'_{WR}\right), \qquad [12]$$

where S_o is the open-circuit selectivity ($V_{WR} = V_{WR}^o$). The above equations, valid for negligible acetaldehyde production, stem directly from the definitions of $\alpha_{C_2H_4O}$ and α_{CO_2} (Eq. [8a]) and contain mathematical information only. They dictate that when the selectivity is at a maximum with respect to V_{WR} (and $e\Phi$) then $\alpha_{C_2H_4O} = \alpha_{CO_2}$. This is indeed the case as shown in Figs. 7b and 8b. The same figures show that when $\alpha_{C_2H_4O} > \alpha_{CO_2}$ then the selectivity increases with V_{WR} as also dictated by Eqs. [11] and [12]. What the above mathematical equations do not necessarily dictate, however, and what is rather surprising and physically interesting is that $\alpha_{C_2H_4O}$ and α_{CO_2} are maximized at the same V_{WR} and $e\Phi$ values as the selectivity does. This implies physically that the *selectivity to ethylene oxide is maximized when the charge transferred between the catalyst and the adsorbed activitated complex in the rate limiting step is maximum and near one.* This is consistent with the idea that covalently bonded oxygen rather than ionic oxygen (which has already accepted up to two electrons from the Ag catalyst) leads to epoxidation.

There is, however, another important feature of Figs. 7b and 8b which seems to challenge the idea of the two intrinsically different chemisorbed types of oxygen (α- and β-), one leading to epoxidation, the other to complete oxidation. If this were exactly the case, then one would expect $\alpha_{C_2H_4O}$ and α_{CO_2} to be consistently and significantly different since the partial charges δ_α^- and δ_β^- (Fig. 16) are expected to differ significantly. In fact, according to the previous paragraph, one would expect to have $\alpha_{C_2H_4O} > \alpha_{CO_2}$ over the entire V_{WR} range. The fact that this is not the case and that $\alpha_{C_2H_4O}$ and α_{CO_2} trace each other so closely, as V_{WR} is varied, leads to an alternative picture: There may exist, as originally proposed by Grant and Lambert (5), only one type of oxygen leading both to epoxidation and complete oxidation. Changing V_{WR}, or adding Cl, simply changes the binding state of this oxygen and thus affects both its reactivity and its relative propensity for epoxidation and complete oxidation. As V_{WR} (and $e\Phi$) is increased the chemisorptive bond weakens and this causes the pronounced increase in both rates (Figs. 7a and 8a). Also as V_{WR} is increased, the partial negative charge of this oxygen varies (to a first approximation as the parameter $2\text{-}\alpha_{C_2H_4O} \approx 2\text{-}\alpha_{CO_2}$) and when this charge is minimum (covalently bonded electrophilic oxygen) then the selectivity to ethylene oxide is maximized (Figs. 7b and 8b). This picture, where the α- and β-oxygen are extreme conformations of the same atomic oxygen species (each predominating at different V_{WR}, $e\Phi$, chlorine coverage, etc.) rather than two separate species which coexist on the surface, appears to be perfectly consistent with the observed dependence of the rates (Figs. 7a, 8a) and of the α coefficients (Figs. 7b, 8b) on catalyst potential and work function.

CONCLUSIONS

The catalytic activity and selectivity of Ag films deposited on O^{2-}-conducting solid electrolytes can be varied markedly and reversibly at temperatures, pressures, and gaseous compositions similar to those used in industrial practice via the effect of NEMCA or *in situ* controlled promotion. The rates of epoxidation and complete oxidation vary by up to a factor of 230 by changing the catalyst potential. The rate changes are typically a factor of 200 higher than the rate of supply or removal of promoting oxide ions. Dramatic variations in product selectivity are also obtained. For negative catalyst potentials, i.e., low work function values, acetaldehyde becomes the main product with selectivity up to 55%. Positive potentials in conjunction with dichloroethane addition lead to ethylene oxide selectivity up to 78%. Increasing catalyst work function, which is *in situ* controlled by the catalyst potential, and addition of dichloroethane cause qualitatively similar effects on the selectivity to ethylene oxide, but a constructive synergy also exists.

Ethylene oxide selectivity is maximized when the NEMCA coefficients α $(=(RT/F)dr/dV_{WR})$ are also at a maximum. This shows that covalently bonded atomic oxygen has a higher propensity for epoxidation. The fact that $\alpha_{C_2H_4O}$ and α_{CO_2} differ only marginally but vary significantly with catalyst potential (roughly between 0 and 1) shows that the same atomic oxygen species is responsible for epoxidation and complete oxidation and that its partial charge, dipole moment, binding strength, and propensity for epoxidation can be affected significantly and controlled by the catalyst potential.

The ability of solid electrolytes to tune precisely and *in situ* the state of catalyst surfaces via NEMCA appears to be of considerable practical importance. It also permits a systematic study of the role of promoters in heterogeneous catalysis.

APPENDIX

Here we derive Eqs. [11] and [12]. We denote $\alpha_{C_2H_4O}=\alpha_1$, $\alpha_{CO_2}=\alpha_2$, $r_{C_2H_4O}=r_1$, $r_{CO_2}=r_2$, and $V_{WR}=V$. From the definitions of the NEMCA coefficients $\alpha_{C_2H_4O}$ and α_{CO_2} (Eq. [8a]) one obtains

$$\frac{F}{RT}(\alpha_1-\alpha_2)\,dV=\frac{dr_1}{r_1}-\frac{dr_2}{r_2}=-\frac{r_1dr_2-r_2dr_1}{r_1r_2}=-\frac{r_1}{r_2}d\left(\frac{r_2}{r_1}\right). \quad [A1]$$

From the definition of the selectivity to ethylene oxide S,

$$S=\frac{r_1}{r_1+r_2}=\frac{1}{1+(r_2/r_1)}, \quad [A2]$$

it follows that

$$dS=-\frac{d(r_2/r_1)}{(1+r_2/r_1)^2}. \quad [A3]$$

Combining [A1] and [A3] one obtains

$$\frac{r_1}{r_2}\left(1+\frac{r_2}{r_1}\right)^2dS=\frac{F}{RT}(\alpha_1-\alpha_2)\,dV, \quad [A4]$$

or, using [A2],

$$\frac{dS}{S(1-S)}=\frac{F}{RT}(\alpha_1-\alpha_2)\,dV, \quad [A5]$$

which is Eq. [11]. Direct integration gives then Eq. [12].

ACKNOWLEDGMENTS

We thank the EEC JOULE and SCIENCE Programmes for financial support and the ICEHT, Patras, for a fellowship to Ch. Karavassilis. Sincerest thanks are also expressed to Prof. R. M. Lambert for numerous helpful discussions.

REFERENCES

1. Kilty, P. A., and Sachtler, W. H., *Catal. Rev. Sci. Eng.* **10**, 1 (1974).
2. Verykios, X. E., Stein, F. P., and Coughlin, R. W., *Cat. Rev. Sci. Eng.* **22**, 197 (1980).
3. Sachtler, W. M. H., Backx, C., and Van Santen, R. A., *Catal. Rev. Sci. Eng.* **23**, 127 (1981).
4. Van Santen, R. A., and Kuipers, H. P. C. E., *in* "Advances in Catalysis" (D. D. Eley, H. Pines, and P. B. Weisz, Eds.), Vol. 35, p. 265. Academic Press, New Yrok, 1987.
5. Grant, R. B., and Lambert, R. M., *J. Catal.* **92**, 364 (1985).
6. Tan, S. A., Grant, R. B., and Lambert, R. M., *J. Catal.* **104**, 156 (1987).
7. Tan, S. A., Grant, R. B., and Lambert, R. M., *J. Catal.* **106**, 54 (1987).
8. Haul, R., and Neubauer, G., *J. Catal.* **105**, 39 (1987).
9. Gleaves, J. T., Sault, A. G., Madix, T. J., and Ebner, J. R., *J. Catal.* **121**, 202 (1990).
10. Carter, E. A., and Goddard, W. A., III, *J. Catal.* **112**, 80 (1988).
11. Van Santen, R. A., and De Groot, C. P. M., *J. Catal.* **98**, 530 (1980).
12. Bukhtiyarov, V. I., Boronin, A. I., and Savchenko, V. I., *J. Catal.* **150**, 262, 268 (1994).
13. Jorgensen, K. A., and Hoffmann, R., *J. Phys. Chem.* **94**, 3046 (1990).
14. Backx, C., De Groot, C. P. M., and Biloen, P., *Surf. Sci.* **104**, 300 (1981).
15. Rovida, G., Pratesi, F., Maglietta, M., and Ferroni, E., *Surf. Sci.* **43**, 230 (1974).
16. Rehren, C., Muhler, M., Bao, X., Schlögl, R., and Ertl, G., *Z. Phys. Chem.* **174**, 11 (1991).
17. Compbell, C. C., and Paffett, M. T., *Surf. Sci.* **143**, 517 (1984).
18. Van den Hoek, P. J., Baerends, E. J., and Van Santen, R. A., *J. Phys. Chem.* **93**, 6469 (1989).
19. Vayenas, C. G., Bebelis, S., and Neophytides, S., *J. Phys. Chem.* **92**, 5083 (1988).
20. Vayenas, C. G., Bebelis, S., and Ladas, S., *Nature (London)* **343**, 625 (1990).
21. Pritchard, J., *Nature (London)* 342, 592 (1990).
22. Vayenas, C. G., Bebelis, S., Yentekakis, I. V., and Lintz, H.-G., *Catal. Today* **11**, 303 (1992).
23. Bebelis, S., and Vayenas, C. G., *J. Catal.* **118**, 125 (1989).
24. Neophytides, S., and Vayenas, C. G., *J. Catal.* **118**, 147 (1989).
25. Vayenas, C. G., and Neophytides, S., *J. Catal.* **127**, 645 (1991).
26. Bebelis, S., and Vayenas, C. G., *J. Catal.* **138**, 588 (1992).
27. Tsiakaras, P., and Vayenas, C. G., *J. Catal.* **140**, 53 (1993).
28. Vayenas, C. G., Bebelis, S., and Despotopoulou, M., *J. Catal.* **128**, 415 (1991).
29. Yentekakis, I. V., and Vayenas, C.G., *J. Catal.* **149**, 238 (1994).
30. Alqahtany, H., Chiang, P. H., Eng, D., and Stoukides, M., *Catal. Lett.* **13**, 289 (1992).
31. Cavalca, C. A., Larsen, G., Vayenas, C. G., and Haller, G. L., *J. Phys. Chem.* **97**, 6115 (1993).
32. Yentekakis, I. V., Moggridge, G., Vayenas, C. G., and Lambert, R. M., *J. Catal.* **146**, 292 (1994).
33. Politova, T. I., Sobyanin, V. A., and Belyaev, V. D., *React. Kinet. Catal. Lett.* **41**, 321 (1990).
34. Mar'ina, O. A., and Sobyanin, V. A., *Catal. Lett.* **13**, 61 (1992).
35. Mar'ina, O. A., and Sobyanin, V. A., Belyaev, V. D., and Parmon, V. N., *Catal. Lett.* **13**, 567 (1992).
36. Varkaraki, E., Nicole, J., Plattner, Comninellis, Ch., and Vayenas, C. G., *J. Appl. Electrochem.* **25**, 978 (1995).
37. Pliangos, C., Yentekakis, I. V., Verykios, X. E., and Vayenas, C. G., *J. Catal.* **154**, 124 (1995).
38. Harkness, I. R., and Lambert, R. M., *J. Catal.* **152**, 211 (1995).
39. Cavalca, C. A., and Haller, G. L., *J. Catal.* in press (1996).
40. Neophytides, S. G., Tsiplakides, D., Stonehert, P., Jaksic, M. M., and Vayenas, C. G., *Nature (London)* **370**, 45 (1994).
41. Bockris, J. O.' M., and Minevski, Z. S., *Electrochim. Acta* **39**(11/12), 1471 (1994).

42. Ladas, S., Kennou, S., Bebelis, S., and Vayenas, C. G., *J. Phys. Chem.* **97**, 8845 (1993).
43. Vayenas, C. G., Jaksic, M. M., Bebelis, S. I., and Neophytides, S. G., The electrochemical activation of catalytic reactions, *in* "Modern Aspects of Electrochemistry" (Bockris, J. O.' M., *et al.*, Eds.), Vol. 29, pp. 57–202. Plenum, New York, 1995.
44. Vayenas, C. G., and Yentekakis, I. V., Electrochemical modification of catalytic activity, *in* "Handbook of Heterogeneous Catalysis" (G. Ertl, H. Knötzinger, and J. Weitkamp, Eds.), VCH, Weinheim/New York. 1996 (in press).
45. Vayenas, C. G., Ladas, S., Bebelis, S., Yentekakis, I. V., Neophytides, S., Jiang Yi, Karavasilis, Ch., and Pliangos, C., *Electrochim. Acta* **39**(11/12), 1849 (1994).
46. Bockris, J. O. 'M., and Reddy, A. K. N., *in* "Modern Electrochemistry" Vol. 2. Plenum, New York, 1970.
47. Stoukides, M., and Vayenas, C. G., *J. Catal.* **70**, 137 (1981).
48. Stoukides, M., and Vayenas, C. G., *ACS Symp. Ser.* **178**, 181 (1992).
49. Karavasilis, Ch., Bebelis, S., and Vayenas, C. G., *J. Catal.,* **160**, 205 (1996).
50. Zomerdijk, J. C., and Hall, M. W. *Catal. Rev. Sci. Eng.* **23**, 163 (1981).
51. Stoukides, M., and Vayenas, C. G., *J. Catal.* **69**, 18 (1981).
52. Karavasilis, Ch., Ph.D. thesis, Univ. of Patras, 1994.
53. Stoukides, M., and Vayenas, C. G., *J. Catal.* **64**, 18 (1980).
54. Bebelis, S., and Vayenas, C. G., *J. Catal.* **138**, 570 (1992).
55. Arakawa, T., Saito, A, and Shiokawa, J., *Chem. Phys. Lett.* **94**, 250 (1983).
56. Arakawa, T., Saito, A., and Shiokawa, J., *Appl. Surf. Sci.* **16**, 365 (1983).
57. U. Vohrer, Ph.D. thesis, Univ. of Tübingen, 1992.
58. Zipprich, W., Wiemhöfer, H.-D., Vohrer, U., and Göpel, W., *Ber. Bunsenges. Phys. Chem.* **99**, 1406 (1995).
59. Ladas, S., Bebelis, S., and Vayenas, C. G., *Surf. Sci.* **251/252**, 1062 (1991).
60. Basini, L., Cavalca, C., Larsen, G., and Haller, G. L., *J. Phys. Chem.* **98**, 10853 (1994).
61. Boudart, M., *J. Am. Chem. Soc.* **74**, 3556 (1952).
62. Bebelis, S., Ph.D. thesis, Univ. of Patras, 1989.
63. Wang, D. Y., and Nowick, A. S., *J. Electrochem. Soc.* **126**, 1155 (1979).
64. Verkerk, M. J., Hammink, M. W. J., and Burggraaf, A. J., *J. Electrochem. Soc.* **130**, 70 (1983).
65. Van Herle, J., and McEvoy, A. J., *J. Phys. Chem. Solids* **55**(4), 339 (1994).
66. Backx, C., Moolhuysen, J., Geenen, P., and Van Santen, R. A., *J. Catal.* **72**, 364 (1981).
67. Plischkle, J. K., Benesi, A. J., and Vannice, M. A., *J. Catal.* **138**, 223 (1992).
68. Fernandes, E. F., Benesi, A. J., and Vannice, M. A., *J. Phys. Chem.* **98**, 8498 (1994).
69. Krüger, B., and Benndorf, C., *Surf. Sci.* **704**, (1986).
70. Schmiedl, E., Wissmann, P., and Wittmann, E., *Surf. Sci.* **135**, 341 (1983).
71. Hölzl, J., and Schulte, F. K. *in* "Solid Surface Physics," pp. 1–150. Springer Verlag, Berlin, 1979.
72. Rodriguez, J. A., and Campbell, C. T., *Surf. Sci.* **206**, 426 (1988).
73. Tan, S. A., Grant, R. B., and Lambert, R. M., *J. Catal.* **100**, 383 (1986).
74. Van Santen, R. A., "Proceedings, 9th International Congress on Catalysis, Calgary, 1988" (M. J. Phillips and M. Tenan, Eds.). Chem. Institute of Canada, Ottawa, 1988.